Contribution of sea-ice albedo and insulation effects to Arctic amplification in the EC-Earth Pliocene simulation

Jianqiu Zheng[1,2,3], Qiong Zhang[1], Qiang Li[1,] Qiang Zhang[1], Ming Cai[4]

[1]Department of Physical Geography and Bolin Centre for Climate Research, Stockholm University, Stockholm, 10691, Sweden
[2]School of Earth and Space Sciences, University of Science and Technology of China, Hefei, 230026, China
[3]Key Laboratory of Meteorological Disaster of Ministry of Education, Nanjing University of Information Science and Technology, Nanjing, 210044, China
[4]Department of Earth, Ocean and Atmospheric Science, Florida State University, Tallahassee, Florida, 32306, USA

Correspondence to: Jianqiu Zheng (qiu@ustc.edu.cn)

Abstract. In the present work, we simulate the Pliocene climate with EC-Earth climate model as an analogue for current warming climate induced by rising CO_2 in the atmosphere. The simulated Pliocene climate shows a strong Arctic amplification featured by pronounced warming sea surface temperature (SST) over North Atlantic in particular over Greenland Sea and Baffin Bays, which is comparable with geological SST reconstructions from PRISM. To understand the underlying physical processes, the air-sea heat flux variation in response to Arctic sea-ice change is quantitatively assessed by a climate feedback and response analysis method (CFRAM) and an equilibrium feedback assessment (EFA)-like approach. Giving the facts that the maximum warming in SST occurs in summer while the maximum warming in surface air temperature happens during winter, our analyses show that dominant ice-albedo effect is the main reason for summer SST warming, a 1% loss in sea-ice concentration could lead to an approximate 2 Wm^{-2} increase in shortwave solar radiation into open sea surface. During winter month, the insulation effect induces enhanced turbulent heat flux out of sea surface due to sea-ice melting in previous summer months. This leads to more heat release from the ocean to atmosphere, thus explaining the stronger surface air temperature warming amplification in winter than in summer.

1 Introduction

Through the monitoring at Mauna Loa Observatory in Hawaii (https://www.esrl.noaa.gov/gmd/obop/mlo/), the CO2 concentration in the atmosphere had steadily passed 400 ppm threshold by September 2016. Accordingly, global mean temperature in 2016 increased about 1.1°C to that of preindustrial as released by the World Meteorological Organization (https://public.wmo.int/en/media/press-release), one major consequence of this continuing and accelerating warming is the rapid melting of ice in high latitudes. Ten lowest minimum Arctic sea-ice extents since satellite records available in 1979 have taken place in recent decade except for 2005, as documented by National Snow and Ice Data Centre. Moreover, ice-free Arctic Ocean is estimated to emerge around 2050 on the basis of climate model projections (Overland et al., 2011). As the sea-ice retreats, its reflectivity and insulation decrease. This leads to the changes in surface heat budget, and the changes in

overlying cloud and water vapour, further amplify the Arctic warming and sea-ice melting. Many studies have shown that the accelerated Arctic sea-ice retreat is possibly resulted from local ice-albedo positive feedback (Winton, 2008), meridional heat transport by atmospheric circulation and oceanic current (Alexeev et al., 2013), or sea-ice drift out of the Fram Strait

35 (Nghiem et al., 2007; Krumpen et al., 2016). In turn, Arctic sea-ice decline can result in a variety of impacts on climate change, such as Arctic amplification (Serreze et al., 2009), change of cloud cover and precipitation (Liu et al., 2012; Bintanja and Selten, 2014), shift in atmospheric circulation pattern (Alexander et al., 2004), and slow-down of the Atlantic Meridional Overturning Circulation (Sévellec et al., 2017). A detailed consequence of Arctic sea-ice decline classified by local and remote effects have been reviewed by Vihma et al. (2014).

40   Such ongoing high CO_2 level and low ice concentration in Arctic is not unique in Earth's history. Geological data show that during the Pliocene the CO_2 concentration in the atmosphere did reach 400 ppm or even more, and extreme warmth and Arctic amplification are recorded in multi-proxy evidence, including the longest and most complete record from Lake El'gygytgyn, an undisturbed Siberian lake in northeast Arctic Russia (Brigham-Grette et al., 2013). Seasonally ice-free conditions existed in some Arctic regions in the mid-Pliocene until the circulation through the Bering Strait reversed and the

45 excess freshwater supply might have facilitated sea-ice formation (Matthiessen et al., 2009). Several climate models have simulated the Pliocene but failed to reproduce the strong Arctic amplification showed in geological proxy data (Dowsett et al., 2012). While most of previous studies on contribution of sea-ice effect to Arctic amplification focus on contemporary trend or future projection, here the Pliocene simulation is selected because of three reasons: (1) The Pliocene epoch (~ 3 million years ago), the most recent warm period with the similar CO_2 concentration as today, is not only an analogue of

50 future climate change but also an appropriate past time-slice to examine sea-ice effect (Haywood et al., 2016a). (2) The Pliocene simulation can be partly verified by proxy data reconstructed from deep-sea oxygen isotope analysis (Dowsett et al., 2012), while the future projection from climate model is of high uncertainty owing to the lack of any validation. (3) Whereas the historical or undergoing climate variability is transient, the Pliocene simulation is obtained after the model integration reaches a quasi-equilibrium state. As inferred from Li et al. (2013), the equilibrium response is in principle

55 reversible while transient response is hysteretic, suggesting that the Pliocene simulation can better represent a steady climate response.

    Two physical attributions of sea-ice are considered to affect climate system. One is much higher surface reflectivity of ice than that of open water, and the other is that ice can inhibit or reduce the exchange of momentum, heat and mass between the atmosphere and ocean, hereafter we refer these two attributions as albedo and insulation effects respectively. Most previous

60 studies on the two effects are mainly carried out by sensitivity experiments with atmospheric general circulation model (AGCM). For instance, Gildor et al. (2014) examined the role of sea-ice on hydrological cycle using the Community Atmospheric General Circulation Model (CAM3). Two effects are separated by modifying the sea-ice albedo to that of open-water or setting the sea-ice thickness to zero but its albedo keeping unchanged. Their results show that the insulation effect on the hydrological cycle is larger than the albedo effect, and these two effects are not independent, i.e. their total effect is

65 not the sum of their separate contribution. Lang et al. (2017) also pointed out that the sea-ice thinning in recent years can

lead to increase 37% of Arctic amplification through the enhanced insulation effect, as estimated by an AGCM. Note that sea surface temperature (SST) is prescribed in their AGCM simulation while sea-ice albedo or thickness is modified. In fact, the modification of sea-ice does not match the fixed SST closely, which may lead to a bias in the sea-ice effect estimation from AGCM simulation. The climate system in turn reinforces sea-ice loss while influenced by albedo or insulation effect, which

70 is known as ice-albedo feedback or ice-insulation feedback. In addition, albedo effect and insulation effect interacts in a nonlinear way (Gildor et al., 2014). These feedbacks and interaction add more challenges to understand the effect of sea-ice on climate. Recently Burt et al. (2016) and Kim et al. (2016) addressed the relationship between sea-ice loss and air-sea interface heat budget using the Community Earth System Model (CESM) simulation and cyclo-stationary empirical orthogonal function (CSEOF) analysis respectively. However, the studies contain large uncertainties due to the hysteresis of

75 transient processes (Li et al., 2013). Although the surface heat budget is the most fundamental to air-sea interaction, it is still not clear to what degree heat flux responds to the change of Arctic sea-ice. Therefore the present study aims to quantitatively assess the variation of each individual component of air-sea heat flux caused by the decrease of Arctic sea-ice albedo and insulation. The analysis is based on the EC-Earth simulation of the Pliocene climate, which representing an analogue for a future equilibrium climate, and the reference state is preindustrial equilibrium climate state.

80 The remainder of the paper is organized as follows. Section 2 describes the EC-Earth model and experimental design, and introduces the climate feedback and response analysis method (CFRAM), as well as the approach to extract the impact contributed from sea-ice loss. In section 3, we present several climate features simulated in the Pliocene experiment. The albedo and insulation effects of sea-ice on air-sea interface heat flux are investigated respectively in sections 4 and 5, followed by summary and discussion in section 6.

85 2 Model and method

2.1 Model description and experimental design

The model applied in the study is global coupled climate model EC-Earth (version 3.1, Hazeleger et al., 2012). Its atmospheric component is the Integrated Forecast System (IFS, version cycle 36r4) developed at the European Centre for Medium-Range Weather Forecast (ECMWF), including the land model H-TESSEL (Balsamo et al., 2009). This atmospheric

90 spectral model is run at T159 resolution (roughly 1.125°, ~125 km) with 62 vertical levels and coupled to the ocean component that is based on the Nucleus for European Modelling of the Ocean (NEMO, version 3.3, Madec, 2008) and the Louvain-la-Neuve sea-ice Model (LIM, version 3, Vancoppenolle et al. 2009). The NEMO is developed at the Institute Pierre Simon Laplace (IPSL) and has a resolution of about 1° and 46 vertical levels. In LIM3, surface albedo parameterization follows Shine and Henderson-Sellers (1985), with thick dry snow 0.8, thick melting snow 0.65, thick

95 frozen bare ice 0.72, thick melting bare ice 0.53, thin melting ice 0.47. The tuning of bare ice and snow albedo would affect whether the equilibrium ice thickness is reasonable and the ice is from a multi-year or seasonal ice zone. The coupling between the atmosphere and ocean/sea-ice is through the Ocean Atmosphere Sea-ice Soil coupler (OASIS, version 3.0,

Valcke, 2006). EC-Earth has been used to examine the Arctic climate for the historical period and future scenarios in CMIP5. An evaluation of EC-Earth for the Arctic shows that the model simulates the 20th century Arctic climate reasonably well. EC-Earth simulated cloud variables with slightly larger cloud fraction and less cloud condensate compared to ERA-Interim, which lead to similar longwave cloud radiative forcing. Moreover, total cloud forcing in EC-Earth is in good agreement to the APP-x satellite estimates (Koenigk et al., 2013). Koenigk et al. (2013) showed that the annual mean surface temperature in Arctic increases by 12 K in the EC-Earth RCP8.5 scenario simulation, and the most pronounced warming is during autumn and winter in the lower atmosphere. A likely ice-free Arctic is indicated in September around 2040. The enhanced oceanic meridional heat flux into the Arctic (Koenigk et al., 2013) and the enhanced atmospheric northward latent energy transport (Graversen and Burtu, 2016) are suggested as major contributors to the future Arctic warming in EC-Earth simulation. Recently the EC-Earth model is also applied to understand the past climate such as the change of Arctic climate (Muschitiello et al., 2015), African monsoon (Pausata et al., 2016; Gaetani et al., 2017), tropical cyclone (Pausata et al., 2017a) and ENSO activity (Pausata et al., 2017b) during mid-Holocene. In this study we apply the model to mid-Pliocene climate and focus on the effects of sea-ice on Arctic climate change.

Two numerical experiments are performed with EC-Earth to facilitate this study. One is the preindustrial control run with 1850 CO_2 concentration of 284.725 ppm, and the other is the mid-Pliocene warm period sensitivity experiment in which the atmospheric CO_2 concentration is set to 400 ppm. Following the protocol of the Pliocene Model Intercomparison Project phase 2 (PlioMIP2, Haywood et al., 2016b), several configurations are modified in the Pliocene simulation: (1) all other trace gases except CO_2, such as CH_4 and N_2O, and aerosols in the Pliocene experiment are specified to be identical to the preindustrial run. (2) Orbit forcing, including eccentricity, obliquity, and precession, remains same with the preindustrial run. (3) Enhanced boundary condition from the Pliocene Research, Interpretation and Synoptic Mapping group (PRISM, Dowsett et al., 2016) are applied in the Pliocene experiment where the land-sea mask, orography, bathymetry, vegetation, soil and ice-sheet are modified accordingly. The integrations of the preindustrial control run and the Pliocene experiment are carried out for 500 years, and it takes approximate 300 years for model to reach equilibrium. From our last 200 years output in the Pliocene simulation (see Figure S1 in the Supplement), the mean top of the atmosphere (TOA) net radiation is about -0.5 Wm^{-2} and its trend is near zero. The trend of mean SST is about 0.027 K/century, which fulfils the PMIP4 criterion that the trend of mean SST should be less than 0.05 K/century (Kageyama et al., 2018). In this study the last 100-year-mean of all variables are used for analysis, and the Pliocene climate anomalies are calculated with respect to the preindustrial control run. The Arctic in the following analysis is defined as the region poleward of 70°N.

2.2 Climate feedback and response analysis method (CFRAM)

Radiative forcing varies as CO_2 concentration increases in the Pliocene experiment, which drives climate system warming. In response to temperature change, factors such as surface albedo, cloud, water vapour and air temperature will adjust and feedback until climate system reaches equilibrium. The contribution from each factor can be quantitatively evaluated by climate feedback analysis. The traditional climate feedback analysis method, such as partial radiative perturbation (PRP)

technique, is based on TOA radiative budget (Wetherald and Manabe, 1988), while the radiative kernel method can be extended to surface and computationally efficient (Soden and Held, 2006; Pithan and Mauritsen, 2014). However, none of them takes individual physical processes into account, particularly non-radiative processes. The climate feedback and response analysis method (CFRAM) proposed by Lu and Cai (2009) overcomes this limitation.

135   CFRAM contains two parts: one is decomposing radiative perturbation into individual contribution from CO_2, surface albedo, cloud, water vapour and air temperature. It is performed by offline calculation using radiative transfer model (Fu and Liou, 1993) with the output from the preindustrial control run and the Pliocene sensitivity experiment. The other part is calculating partial temperate perturbation due to individual radiative and non-radiative feedback processes, which is based on total energy balance and derived from the relationship between longwave radiation and temperature change. A more detailed
140   description about CFRAM can be found in Lu and Cai (2009).

CFRAM is a practical diagnostic tool to analyze the role of various forcing and feedback agents and has been used widely in climate change research (e.g. Taylor et al., 2013; Song and Zhang, 2014; Hu et al., 2017). In the present study, we apply the first part of CFRAM to obtain the surface radiative flux due to albedo, cloud and water vapour, and link it to albedo or insulation effect of sea-ice.

145   **2.3 Approach to extract sea-ice effects**

As sea-ice declines in the Pliocene warming climate, heat flux at air-sea interface varies. However, the variation is not only due to the impact of sea-ice but also determined by other factors, such as atmospheric circulation. Therefore an approach is indispensable to extract the corresponding part of sea-ice effect from the total heat flux change. To distinguish sea-ice contribution from the other processes, the linkage between sea-ice and heat flux needs to be identified through either
150   temporal correlation or spatial correlation if the effect of sea-ice is assumed to be linear. A canonical case of the former is the equilibrium feedback assessment (EFA) method, which has been used to quantify the influence of sea-ice on cloud cover (Liu et al., 2012) and the heat flux response to SST (Frankignoul and Kestenare, 2002).

Here we adopt a method similar to EFA but built on spatial correlation due to the limitation of data and computation. This method is used in Hu et al. (2017) to correct cloud feedback. The response of heat flux to change in sea-ice concentration
155   (SIC) is represented as

$$F(s) = \lambda I(s) + N(s), \quad (1)$$

where $F(s)$ is the heat flux anomaly at location s, $I(s)$ is anomalous SIC, λ is the response coefficient of heat flux to SIC change, and $N(s)$ is the climate noise independent of SIC variability. The response coefficient can be calculated as

$$\lambda = \frac{cov[F(s), I(s)]}{cov[I(s), I(s)]}, \quad (2)$$

160   where $cov\big[F(s),I(s)\big]$ is the spatial covariance between heat flux and SIC, and $cov\big[I(s),I(s)\big]$ is the spatial variance of

SIC.

The statistical significance of response coefficient is tested using a two-sided Student's t-test, where the effective degree

of freedom is estimated from the auto-correlation function (Bretherton et al., 1999) as

$$n = N\frac{1-r_1 r_2}{1+r_1 r_2}, \quad (3)$$

165   where n is the effective degree of freedom, N is sample size, and r_1 is the lag-one auto-correlation of heat flux and similarly

r_2 for SIC. Note that auto-correlation of heat flux and SIC is so strong that r_1 and r_2 can approach 1, leading to a drastically

decrease of effective degree of freedom.

3 Mid-Pliocene climate features

Unlike the present earth observation system, the Pliocene climate proxy data are reconstructed mainly from the benthic
170   oxygen isotope analysis of deep-sea samples, such as forminifera, diatom and ostracod assemblages. Several climate features
have been revealed with the multi-proxy data, one of the most concern is permanent El Niño-like condition during the mid-
Pliocene warm period (Wara et al., 2005; Federov et al, 2006), which points out that the SST difference between the western
and eastern equatorial Pacific was absent or less evident, similar to the contemporary El Niño SST pattern while not
happening on interannual timescale. The other characteristic is Arctic amplification — the warming in surface air
175   temperature (SAT) in the Arctic region tends to be more than twice as warm as that in the low- and mid-latitude region
(Serreze and Barry, 2011). However, the Arctic SAT and SST during Pliocene is significantly warmer than today even
though they have comparable CO_2 concentration (Ballantyne et al., 2013), which probably stems from the present transient
process that has not yet reached a steady state or is due to the change of the gateways that can affect the Atlantic meridional
overturning circulation (AMOC) (Brierley and Fedorov, 2016).
180   In Figure 1 we show the changes in SST and SAT between the preindustrial period and the Pliocene epoch. The shaded
circles in the SST change distribution (Figure 1a) represent the mean annual SST anomalies at 95% confidence-assessed
marine sites from Deep Sea Drilling Project (DSDP) and Ocean Drilling Program (ODP), which are available in the
supplementary table of Dowsett et al. (2012). In contrast to the underestimation of multi-model ensembles to the warming
over the northern Atlantic sector of the Arctic Ocean (Dowsett et al., 2012), the warming amplitude and pattern in EC-Earth
185   simulation is comparable with the high-confidence proxy data. This is consistent with the results of Koenigk et al. (2013),
which pointed out that the sea ice change in EC-Earth is strong and EC-Earth simulations show a strong Arctic amplification
compared to most CMIP3 models. Meanwhile, a warming can be seen along the coastal upwelling zones off the America,
which implies a permanent El Niño-like feature. According to Figure 1b, the Pliocene SAT north of 70°N is as much as 10-
18°C higher than the preindustrial, similar to mid-Pliocene paleoclimate estimate by Robinson et al. (2008).

190   Figure 1a and 1b also show that the SST and SAT anomaly patterns are somewhat similar over low- and mid-latitude region, but they are apparently different over high latitude region, particularly over the Arctic Ocean, which is previously illustrated by Hill et al. (2014). This disparity results from the intense air-sea coupling over tropical and subtropical ocean, while the air-sea interaction is relatively weak over the Arctic Ocean owing to the albedo and insulation effects of sea-ice. Noteworthily, the warming of SST averaged over the Arctic Ocean shows a distinct seasonal evolution from that of SAT,

195   and the maximum warming in SST occurs in summer while the maximum warming in SAT happens during winter (Figure 1c and 1d).

The SIC is very sensitive during the different period as shown in Figure 2a-c. During the preindustrial the annual mean sea-ice appears to cover the whole Arctic Ocean except for the Greenland Sea, Norwegian Sea and Barents Sea, and it retreats to the western Arctic Ocean in the Pliocene, leading to a significant decrease of sea-ice extent over the Fram Basin

200   and Baffin Bay. Consequently, the net air-sea interface heat exchange varies greatly (Figure 2d-f). The sea-ice covered area seems to be net heat loss during both the preindustrial and the Pliocene. Thus, it can be expected that net heat gain will occur when the sea-ice declines. However, the Fram Basin and Baffin Bay displays pronounced heat loss, which might be linked to the disappearance of sea-ice in the Pliocene (Figure 2b).

The net heat flux at the air-sea interface can be written as

205    $$Q_{net} = Q_{sw} + Q_{lw} + Q_{sh} + Q_{lh}, \quad (4)$$

Where Q_{sw} and Q_{lw} are the net solar shortwave and longwave radiative heat fluxes, Q_{sh} and Q_{lh} are the turbulent sensible and latent heat fluxes. All terms are defined positive downward. Therefore, the positive value means that ocean gains heat from the atmosphere and the negative value means oceanic heat loss.

Figure 3 compares the four components of surface heat flux to further illustrate the possible relationship between sea-ice

210   and net heat exchange (Figure 2c and 2f). The radiative and turbulent heat fluxes both are positive over the Chukchi Sea, thereby marked net heat gain emerging there. Over the Beaufort Sea and East Siberian Sea, the positive shortwave radiation is dominant over the other three negative components, yielding the net heat gain. On the contrary, the positive shortwave radiation over the Fram Basin, Greenland Sea and Baffin Bay is less than the sum of longwave radiation and turbulent heat fluxes, thus leading to net heat loss. The negative turbulent heat fluxes over Fram Basin, Greenland Sea and Baffin Bay are

215   so prominent, indicating the sea-ice effect on turbulent heat fluxes in light of the transition to ice-covered or ice-free state respectively. As shown in Figure 2c, the diagonal stripe represents the region with the transition from ice-covered to ice-free condition, and the diagonal crosshatch represents the region remaining its ice-covered status as the simulation shifts from the preindustrial to the Pliocene.

4 Albedo effect of sea-ice

220   Arctic amplification has been demonstrated in the foregoing Pliocene simulation, and it can be accounted as the synergy of CO_2 external forcing and feedback effects associated with surface albedo, cloud, water vapour and air temperature. That is to

say, the albedo effect of sea-ice and snow can be quantified by climate feedback analysis such as CFRAM. The surface albedo is defined as the ratio of the reflected to the incoming solar shortwave radiation, therefore indicating that albedo effect is relevant with shortwave radiation rather than longwave radiation and turbulent heat fluxes.

225   The annual mean shortwave radiation change due to sea-ice and snow albedo derived from CFRAM is presented in Figure 4. The largest shortwave radiation change exceeding 50 Wm^{-2} takes place over the Fram Basin and Baffin Bay, and most of the Arctic Ocean except for part of North Atlantic and the Barents Sea show shortwave radiative heat gain. Comparing with the SIC change (Figure 2c), the increase of shortwave radiation absorbed by the ocean is in accordance with sea-ice retreat, which can be clearly depicted in scatter plot (Figure 5). The high correlation coefficient (r=-0.92) indicates that sea-ice
230   extent can explain the approximate 84% (square of correlation coefficient) variance of total shortwave radiation change due to albedo, and the residual variance may be caused by snow cover or sea-ice thickness. The statistically significant response coefficient calculated according to formula (2) is -46.5 Wm^{-2} (exceeding 99% confidence level), indicating that 1% decrease in annual mean SIC leads to an approximate 0.5 Wm^{-2} increase in shortwave radiative heat flux at the surface.

        Regarding the seasonal variation of SIC and the incoming solar radiation are distinct in polar region, we examine the
235   response of shortwave radiation to sea-ice change for every month. As shown in Figure 6, the response coefficient of albedo to SIC displays a seasonal variation, in which it peaks in May with the maximum absolute value 188.1 Wm^{-2} (approximate 2 Wm^{-2} increase in shortwave radiation due to 1% decrease in SIC). The prominent oceanic heating in May and June seems inconsistent with the maximum SST warming in August, as the response of seawater lags about 2 months due to the great heat inertia and heat capacity of seawater (Venegas et al., 1997; Zheng et al., 2014). Even though Arctic sea-ice itself has a
240   great variability owing to melting and freezing processes, the SIC anomalies do not exhibit a large variability in different seasons, ranging from 0.34 to 0.44 as shown in the standard deviation of SIC (Table 1). However, the standard deviation of shortwave radiation anomalies associated with albedo effect varies from 88.43 Wm^{-2} in May to 0 Wm^{-2} in December, when the polar night occurring without any sunlight. Moreover, it is found from correlation analysis that sea-ice has a statistically significant impact on surface shortwave radiation except in November, December and January when there is low incident
245   solar shortwave radiation during Arctic winter. Overall, the seasonality of albedo effect of sea-ice on surface shortwave radiation is attributed primarily to seasonal cycle of shortwave radiation, and the contribution of sea-ice variation is substantially small.

5 Insulation effect of sea-ice

5.1 Insulation effect of sea-ice on surface radiation

250   The insulation of sea-ice, separating the overlying atmosphere from the ocean, does not affect surface shortwave or longwave radiation directly. In fact, the insulation reduces the evaporation from the ocean to atmosphere, resulting in a decrease of water vapour and cloud cover, and thus playing a non-negligible role on surface radiation. However, the water vapour and cloud contain a mixture of local evaporation and remote moisture transport. In order to address the insulation

effect of sea-ice, two steps have to be performed. First, we obtain the total influence of water and cloud on surface radiation
255   by CFRAM. Second, we need to extract the contribution from local source associated with sea-ice.

Figure 7 shows the annual mean cloud feedback and water vapour feedback on shortwave and longwave radiation
respectively. Even though the increase in cloud cover is expected with the diminishing Arctic sea-ice (Liu et al., 2012),
whether the increased cloud cover will heat or cool the surface depends on the characteristics of cloud. The cloud feedback
on shortwave radiation is nearly out of phase with that on longwave radiation except in the Beaufort Sea and East Siberian
260   Sea (Figure 7a, 7b). In contrast, the water vapour feedback tends to cool the surface by absorbing solar radiation and heat the
surface by downwelling longwave radiation, and the latter heating is one order of magnitude higher than the former cooling
(Figure 7c, 7d).

The approach to extract the counterpart of sea-ice insulation is based on the premise that the insulation effect on surface
radiation is linear with SIC. Like the steps performed in albedo effect, the response coefficient of shortwave and longwave
265   radiation due to cloud and water vapour for annual mean and seasonal evolution can be calculated respectively, and the
results are shown in Figure 8. As to annual mean, the main contributor comes from cloud feedback on longwave radiation (-
12.6 Wm^{-2}), and the cloud feedback on shortwave radiation and water vapour feedback on longwave radiation are similar in
magnitude but opposite in sign. In addition, the annual mean absorption of incoming solar radiation by water vapour is
negligible, and this is true for the individual month as well. The absorption and reflection of shortwave radiation by cloud
270   represents pronounced seasonal cycle, with large effect in July and August. However, there is no statistically significant
relationship between SIC and cloud feedback on shortwave radiation (Table 2). Comparing the seasonal variation of
shortwave radiation change, standard deviation of longwave radiation caused by cloud and water vapour both show smaller
seasonal variation, therefore leading to a relatively constant contribution of sea-ice insulation to surface longwave radiation
except in summer months when lack of significant interaction between SIC and longwave radiation (Table 2).

275   **5.2 Insulation effect of sea-ice on turbulent heat fluxes**

The air-sea turbulent heat fluxes, including sensible and latent heat fluxes, have been widely studied with bulk aerodynamic
formula, which specifies that the turbulent heat fluxes are dependent on surface wind speed, sea surface and air temperature
difference, specific humidity difference, and bulk heat transfer coefficient. However, due to the existence of sea-ice, the
Arctic turbulent heat fluxes show distinctive features from ice-free condition, which has been mentioned in Section 3. It is
280   therefore essential to take insulation effect of sea-ice into account and differentiate ice-covered flux from ice-free one. This
is demonstrated in Figure 9, which displays the sensible and latent heat flux change as a function of SIC. There are larger
spreads of the turbulent heat flux change over ice-free area than that of ice-covered, because the former is free from the
constraint of sea-ice. The constraint of sea-ice can be apparently captured through the scatter plot of turbulent heat flux and
SIC change (the light blue plot in Figure 9, corresponding to the diagonal crosshatch areas in Figure 2c), and SIC can explain
285   approximate 59% and 74% of the variance in the sensible heat flux and latent heat flux respectively.

The response coefficient of sensible heat flux (35.3 Wm^{-2}) to SIC is larger than that of latent heat flux (27.7 Wm^{-2}), which means that the sensible heat flux is more sensitive to SIC change than the latent heat flux. Noteworthily, this is different from the turbulent heat flux variability over low- and mid-latitude regions, where the trend of sensible heat flux is significantly less than that of latent heat flux (e.g., Li et al., 2011). The positive intercept on the turbulent flux axis implies

290 more heat gain at the sea surface even if there is no SIC change. Because the large specific heat capacity of seawater leads to less warming of the ocean than atmosphere, therefore the sea surface and air temperature difference or specific humidity difference decreases in cold season when the turbulent heat transport is the most pronounced, and consequently resulting in the less heat loss from the ocean to atmosphere.

Figure 10 shows the seasonal response coefficient of the sensible and latent heat fluxes to the sea-ice. Apparently two

295 turbulent heat fluxes have the similar seasonal evolution, peaking in November and showing negative response in July. Therefore the maximum warming of SAT occurs in November as a consequence of atmospheric prompt response to turbulent heating. The melting of sea-ice can attenuate the insulation effect and result in more heat transfer through the processes of conduction or evaporation from the ocean to the atmosphere when SST is higher than SAT, therefore the turbulent heat fluxes correlate positively with SIC in all seasons except summer (Table 3). If SAT is higher than SST, for

300 instance, in July the sea-ice will inhibit the heat transfer from the atmosphere to ocean, thus the negative correlation emerges. However, the correlations between the turbulent heat fluxes and SIC in summer are not statistically significant (Table 3), indicating other factors might be dominant rather than sea-ice.

6 Summary and discussion

In the present work we attempt to understand the albedo and insulation effects of sea-ice, on a warm Arctic climate during

305 Pliocene simulated by EC-Earth coupled model. In contrast to multi-model ensembles documented in Dowsett et al. (2012), the EC-Earth Pliocene simulation can better display some main features manifested in the paleoclimate proxy data from deep-sea oxygen isotope analysis. Arctic amplification in Pliocene had been confirmed by reconstructed data (e.g. Robinson et al., 2008; Brigham-Grette et al., 2013). Proxy data, however, tell only part of the story. Thus a model is applied and it can reveal the complete picture with reasonable explanation.

310 As a key to reveal the important features of Arctic amplification, the air-sea heat flux variation in response to Arctic sea-ice change is quantitatively assessed by CFRAM and an EFA-like method. Table 4 summarizes the results presented in section 4 and 5, which separately illustrated the effects of albedo and insulation of sea-ice on surface heat exchange. Annual mean and seasonal evolution of effects are both considered, and the results are merely the contribution from sea-ice change and expected to partly interpret the variability of heat flux.

315 The albedo only regulates the shortwave radiation, and its effect is primarily determined by annual cycle of insolation. As sea-ice melts from early spring, the enhanced insolation through open sea surface makes the ocean warmer, with the most pronounced heating in May and June. Because of the great heat inertia and heat capacity of seawater, SST warming peaks in August. As a result of albedo effect of sea-ice, ocean heat content increases and more heat is stored in the upper ocean,

which is the potential for the later enhanced heat release from ocean to atmosphere. The insulation effect of sea-ice can
320 modulate not only shortwave and longwave radiation indirectly through cloud and water vapour, but also sensible and latent
heat fluxes directly since sea-ice serves as a barrier. Averaged over the year, the absorption of longwave radiation due to
insulation effect is about 4 times stronger than the reflected shortwave radiation by cloud, while the contribution of water
vapour to shortwave radiation is almost negligible. The longwave radiation change in response to cloud and water vapour is
attributed to downwelling longwave radiation as upwelling longwave radiation depends solely on the surface temperature
325 according to the Stefan–Boltzmann law, and its seasonal variation is relatively small compared to the significant seasonality
showing in shortwave radiation. The sea-ice decline accelerates the turbulent exchange between the ocean and atmosphere,
and the annual sum of sensible and latent heat fluxes exceed radiation fluxes. In particular, heat is released to the atmosphere
by the prominent enhanced turbulent heat fluxes in winter, amplifying the atmospheric warming.

Though significant albedo and insulation effects of sea-ice have been studied, the possible nonlinear response of heat flux
330 to sea-ice can not be captured in this work. In addition, the approach to extract sea-ice effects is based on the spatial
correlation, whether the corresponding conclusion is consistent with that from EFA method remains uncertain. The
consistency check is computationally expensive for CFRAM calculation as the EFA requires high temporal resolution. The
present study is based on the Pliocene simulation with the EC-Earth, and the results may be model dependent. Further work
is needed to compare our results with other PlioMIP models.

335

References

Alexander, M.A., Bhatt, U.S., Walsh, J.E., Timlin, M.S., Miller, J.S. and Scott, J.D.: The atmospheric response to realistic
Arctic sea ice anomalies in an AGCM during winter, J. Climate, 17, 890-905, doi:10.1175/1520-
0442(2004)017<0890:TARTRA>2.0.CO;2, 2004.
345 Alexeev, V.A., Ivanov, V.V., Kwok, R. and Smedsrud, L.H.: North Atlantic warming and declining volume of arctic sea ice,
The Cryosphere Discussions, 7, 245-265, doi:10.5194/tcd-7-245-2013, 2013.
Ballantyne, A.P., Axford, Y., Miller, G.H., Otto-Bliesner, B.L., Rosenbloom, N. and White, J.W.: The amplification of
Arctic terrestrial surface temperatures by reduced sea-ice extent during the Pliocene, Palaeogeogr. Palaeoclimatol.
Palaeoecol., 386, 59-67, doi:10.1016/j.palaeo.2013.05.002, 2013.
350 Balsamo, G., Beljaars, A., Scipal, K., Viterbo, P., van den Hurk, B., Hirschi, M. and Betts, A.K.: A revised hydrology for the

ECMWF model: Verification from field site to terrestrial water storage and impact in the Integrated Forecast System, J. Hydrometeorol., 10, 623-643, doi:10.1175/2008JHM1068.1, 2009.

Bintanja, R. and Selten, F.M.: Future increases in Arctic precipitation linked to local evaporation and sea-ice retreat, Nature, 509, 479-482, doi:10.1038/nature13259, 2014.

355   Bretherton, C.S., Widmann, M., Dymnikov, V.P., Wallace, J.M. and Bladé, I.: The effective number of spatial degrees of freedom of a time-varying field, J. Climate, 12, 1990-2009, doi:10.1175/1520-0442(1999)012<1990:TENOSD>2.0.CO;2, 1999.

Brierley, C. M. and Fedorov, A. V.: Comparing the impacts of Miocene–Pliocene changes in inter-ocean gateways on climate: Central American Seaway, Bering Strait, and Indonesia, Earth Planet. Sci. Lett., 444, 116-130,
360   doi:10.1016/j.epsl.2016.03.010, 2016.

Brigham-Grette, J., Melles, M., Minyuk, P., Andreev, A., Tarasov, P., DeConto, R. and Haltia, E.: Pliocene warmth, polar amplification, and stepped Pleistocene cooling recorded in NE Arctic Russia. Science, 340, 1421, doi:10.1126/science.1233137, 2013.

Burt, M.A., Randall, D.A. and Branson, M.D.: Dark warming, J. Climate, 29, 705-719, doi:10.1175/JCLI-D-15-0147.1,
365   2016.

Dowsett, H.J., Robinson, M.M., Haywood, A.M., Hill, D.J., Dolan, A.M., Stoll, D.K., Abe-Ouchi, A., Chandler, M.A., Rosenbloom, N.A., Otto-Bliesner, B.L. and Bragg, F.J.: Assessing confidence in Pliocene sea surface temperatures to evaluate predictive models, Nat. Clim. Change, 2, 365-371, doi:10.1038/nclimate1455, 2012.

Dowsett, H., Dolan, A., Rowley, D., Moucha, R., Forte, A. M., Mitrovica, J. X., Pound, M., Salzmann, U., Robinson, M.,
370   Chandler, M., Foley, K., and Haywood, A.: The PRISM4 (mid-Piacenzian) paleoenvironmental reconstruction, Clim. Past, 12, 1519-1538, doi:10.5194/cp-12-1519-2016, 2016.

Fedorov, A.V., Dekens, P.S., McCarthy, M., Ravelo, A.C., Barreiro, M., Pacanowski, R.C. and Philander, S.G.: The Pliocene paradox (mechanisms for a permanent El Niño), Science, 312, 1485-1489, doi:10.1126/science.1122666, 2006.

Frankignoul, C. and Kestenare, E.: The surface heat flux feedback. Part I: estimates from observations in the Atlantic and the
375   North Pacific, Clim. Dynam., 19, 633-647, doi:10.1007/s00382-002-0252-x, 2002.

Fu, Q. and Liou, K.N.: Parameterization of the radiative properties of cirrus clouds, J. Atmos. Sci., 50, 2008–2025, doi:10.1175/1520-0469(1993)050<2008:POTRPO>2.0.CO;2, 1993.

Gaetani, M., Messori G., Zhang Q., Flamant C., and Pausata F.S.: Understanding the mechanisms behind the northward extension of the West African Monsoon during the Mid-Holocene. J. Climate, doi:10.1175/JCLI-D-16-0299.1, 2017.

380   Gildor, H., Ashkenazy, Y., Tziperman, E. and Lev, I.: The role of sea ice in the temperature-precipitation feedback of glacial cycles, Clim. Dynam., 43, 1001-1010, doi:10.1007/s00382-013-1990-7, 2014.

Graversen, R.G. and Burtu, M.: Arctic amplification enhanced by latent energy transport of atmospheric planetary waves, Q. J. Roy. Meteor. Soc., 142, 2046-2054, doi:10.1002/qj.2802, 2016.

Haywood, A.M., Dowsett, H.J. and Dolan, A.M.: Integrating geological archives and climate models for the mid-Pliocene

385   warm period, Nat. Commun., 7, 1-14, doi:10.1038/ncomms10646, 2016a.

Haywood, A.M., Dowsett, H.J., Dolan, A.M., Chandler, M.A., Hunter, S.J. and Lunt, D.J.: The Pliocene Model
       Intercomparison Project (PlioMIP) Phase 2: scientific objectives and experimental design, Clim. Past, 12, 663-675,
       doi:10.5194/cp-12-663-2016, 2016b.

Hazeleger, W., Wang, X., Severijns, C., Ştefănescu, S., Bintanja, R., Sterl, A., Wyser, K., Semmler, T., Yang, S., Van den
390   Hurk, B. and Van Noije, T.: EC-Earth V2. 2: description and validation of a new seamless earth system prediction model,
       Clim. Dynam., 39, 2611-2629, doi:10.1007/s00382-011-1228-5, 2012.

Hill, D.J., Haywood, A.M., Lunt, D.J., Hunter, S.J., Bragg, F.J., Contoux, C., Stepanek, C., Sohl, L., Rosenbloom, N.A.,
       Chan, W.L. and Kamae, Y.: Evaluating the dominant components of warming in Pliocene climate simulations, Clim. Past,
       10, 79-90, doi:10.5194/cp-10-79-2014, 2014.

395   Hu, X., Li, Y., Yang, S., Deng, Y. and Cai, M.: Process-based Decomposition of the Decadal Climate Difference between
       2002-13 and 1984-95, J. Climate, 30, 4373-4393, doi:10.1175/JCLI-D-15-0742.1, 2017.

Kageyama, M., Braconnot, P., Harrison, S. P., Haywood, A. M., Jungclaus, J. H., Otto-Bliesner, B. L., Peterschmitt, J.-Y.,
       Abe-Ouchi, A., Albani, S., Bartlein, P. J., Brierley, C., Crucifix, M., Dolan, A., Fernandez-Donado, L., Fischer, H.,
       Hopcroft, P. O., Ivanovic, R. F., Lambert, F., Lunt, D. J., Mahowald, N. M., Peltier, W. R., Phipps, S. J., Roche, D. M.,
400   Schmidt, G. A., Tarasov, L., Valdes, P. J., Zhang, Q., and Zhou, T.: The PMIP4 contribution to CMIP6 – Part 1: Overview
       and over-arching analysis plan, Geosci. Model Dev., 11(3), 1033-1057, doi:10.5194/gmd-11-1033-2018, 2018.

Kim, K.Y., Hamlington, B.D., Na, H. and Kim, J.: Mechanism of seasonal Arctic sea ice evolution and Arctic amplification,
       The Cryosphere, 10(5), 2191-2202, doi:10.5194/tc-10-2191-2016, 2016.

Koenigk, T., Brodeau, L., Graversen, R. G., Karlsson, J., Svensson, G., Tjernström, M. and Wyser, K.: Arctic climate change
405   in 21st century CMIP5 simulations with EC-Earth, Climate dynamics, 40(11-12), 2719-2743, doi: 10.1007/s00382-012-
       1505-y, 2013.

Krumpen, T., Gerdes, R., Haas, C., Hendricks, S., Herber, A., Selyuzhenok, V., Smedsrud, L. and Spreen, G.: Recent
       summer sea ice thickness surveys in Fram Strait and associated ice volume fluxes, The Cryosphere, 10, 523-534,
       doi:10.5194/tc-10-523-2016, 2016.

410   Lang, A., Yang, S. and Kaas, E.: Sea-ice thickness and recent Arctic warming, Geophys. Res. Lett., 44, 409-418,
       doi:10.1002/2016GL071274, 2017.

Li, C., Notz, D., Tietsche, S. and Marotzke, J.: The transient versus the equilibrium response of sea ice to global warming,
       J.Climate, 26, 5624-5636, doi:10.1175/JCLI-D-12-00492.1, 2013.

Li, G., Ren, B., Zheng, J. and Yang, C.: Net air–sea surface heat flux during 1984–2004 over the North Pacific and North
415   Atlantic oceans (10N–50N): annual mean climatology and trend, Theor. Appl. Climatol., 104, 387-401, doi:
       10.1007/s00704-010-0351-2, 2011.

Liu, Y., Key, J.R., Liu, Z., Wang, X. and Vavrus, S.J.: A cloudier Arctic expected with diminishing sea ice, Geophys. Res.
       Lett., 39, L05705, doi:10.1029/2012GL051251, 2012.

Lu, J. and Cai, M.: A new framework for isolating individual feedback processes in coupled general circulation climate

420   models. Part I: Formulation, Clim. Dynam., 32, 873–885, doi:10.1007/s00382-008-0425-3, 2009.

Madec, G.: ''NEMO ocean engine''. Note du Pole de mode ´lisation, Institut Pierre-Simon Laplace (IPSL), France, No 27
        ISSN no 1288-1619, 2008.

Matthiessen, J., Knies, J., Vogt, C. and Stein, R.: Pliocene palaeoceanography of the Arctic Ocean and subarctic seas, Philos.
        Trans. R. Soc. A., 367, 21–48, doi: 10.1098/rsta.2008.0203, 2009.

425   Muschitiello, F., Zhang, Q., Sundqvist, H.S., Davies, F.J. and Renssen, H.: Arctic climate response to the termination of the
        African Humid Period, Quat. Sci. Rev., 125, 91-97, doi:10.1016/j.quascirev.2015.08.012, 2015.

Nghiem, S.V., Rigor, I.G., Perovich, D.K., Clemente-Colón, P., Weatherly, J.W. and Neumann, G.: Rapid reduction of
        Arctic perennial sea ice, Geophys. Res. Lett., 34, L19504, doi:10.1029/2007GL031138, 2007.

Overland J.E., Wang M., Walsh J.E., Christensen J.H., Kattsov V.M., Champan W.L.: Climate model projections for the

430   Arctic. In: AMAP (2011) Snow, Water, Ice and Permafrost in the Arctic (SWIPA): Climate Change and the Cryosphere.
        Arctic Monitoring and Assessment Programme (AMAP), Oslo, Norway. Xii, 538 pp , 2011.

Pausata, F.S., Messori, G. and Zhang, Q.: Impacts of dust reduction on the northward expansion of the African monsoon
        during the Green Sahara period, Earth Planet. Sci. Lett., 434, 298-307, doi:10.1016/j.epsl.2015.11.049, 2016.

Pausata, F.S., Emanuel, K.A., Chiacchio, M., Diro, G.T., Zhang, Q., Sushama, L., Stager, J.C. and Donnelly, J.P.: Tropical

435   cyclone activity enhanced by Sahara greening and reduced dust emissions during the African Humid Period, Proc. Natl.
        Acad. Sci., 114, 6221-6226, doi:10.1073/pnas.1619111114, 2017a.

Pausata, F.S., Zhang, Q., Muschitiello, F., Lu, Z., Chafik, L., Niedermeyer, E.M., Stager, J.C., Cobb, K.M. and Liu, Z.:
        Greening of the Sahara suppressed ENSO activity during the mid-Holocene, Nat. Commun., *8*, 1-12,
        doi:10.1038/ncomms16020, 2017b.

440   Pithan, F. and Mauritsen, T.: Arctic amplification dominated by temperature feedbacks in contemporary climate models,
         Nat. Geosci., 7, 181-184, doi:10.1038/ngeo2071, 2014.

Robinson, M.M., Dowsett, H.J. and Chandler, M.A.: Pliocene role in assessing future climate impacts, EOS, Trans. Am.
         Geophys. Union, 89, 501-502, doi:10.1029/2008EO490001, 2008.

Serreze, M.C., Barrett, A.P., Stroeve, J.C., Kindig, D.N. and Holland, M.M.: The emergence of surface-based Arctic

445   amplification, The Cryosphere, 3, 11-19, doi:10.5194/tc-3-11-2009, 2009.

Serreze, M.C. and Barry, R.G.: Processes and impacts of Arctic amplification: A research synthesis, Glob. Planet. Chang.,
        77, 85-96, doi:10.1016/j.gloplacha.2011.03.004, 2011.

Sévellec, F., Fedorov, A.V. and Liu, W.: Arctic sea-ice decline weakens the Atlantic Meridional Overturning Circulation,
        Nat. Clim. Change, 7, 604-610, doi:10.1038/nclimate3353, 2017.

450   Shine, K.P. and Henderson-Sellers, A.: The sensitivity of a thermodynamic sea ice model to changes in surface albedo
        parameterization. Journal of Geophysical Research, 90, 2243–2250, 1985.

Soden, B. J. and Held, I. M.: An assessment of climate feedbacks in coupled ocean–atmosphere models, J. Climate, 19,

    3354–3360, doi:10.1175/JCLI3799.1., 2006.

Song, X. and Zhang, G.J.: Role of climate feedback in El Niño–like SST response to global warming, J. Climate, *27*, 7301-

455   7318, doi:10.1175/JCLI-D-14-00072.1, 2014.

Taylor, P.C., Cai, M., Hu, A., Meehl, J., Washington, W. and Zhang, G.J.: A decomposition of feedback contributions to
    polar warming amplification. J. Climate, 26, 7023-7043, doi:10.1175/JCLI-D-12-00696.1, 2013.

Valcke, S.: OASIS3 user guide (prism_2-5), PRISM report series, no 2, 6th edn., 2006.

Vancoppenolle, M., Fichefet T., Goosse H., Bouillon S., Madec G. and Maqueda M. A.: Simulating the mass balance and

460   salinity of Arctic and Antarctic sea ice. 1. Model description and validation, Ocean Modelling, 27, 33-53,
    doi:10.1016/j.oceamod.2008.10.005., 2009.

Venegas, S. A., Mysak, L. A. and Straub, D. N.: Atmosphere–ocean coupled variability in the South Atlantic. J.
    Climate, 10(11), 2904-2920, doi:10.1175/1520-0442(1997)010<2904:AOCVIT>2.0.CO;2, 1997.

Vihma, T.: Effects of Arctic sea ice decline on weather and climate: a review. Surv. Geophys., 35, 1175-1214,

465   doi:10.1007/s10712-014-9284-0, 2014.

Wara, M.W., Ravelo, A.C. and Delaney, M.L.: Permanent El Niño-like conditions during the Pliocene warm period. Science,
    309, 758-761, doi:10.1126/science.1112596, 2005.

Wetherald, R. T. and Manabe S.: Cloud feedback processes in a general circulation model. J. Atmos. Sci., 45, 1397–1416,
    doi:10.1175/1520-0469(1988)045,1397:CFPIAG.2.0.CO;2., 1988.

470   Winton, M.: Sea ice–albedo feedback and nonlinear Arctic climate change. Arctic sea ice decline: Observations, projections,
    mechanisms, and implications, 111-131, doi:10.1029/180GM09, 2008.

Zheng, J., Ren, B., Li, G. and Yang, C.: Seasonal dependence of local air-sea interaction over the tropical Western Pacific
    warm pool. J. Trop. Meteorol., 20(4), 360-367, doi:10.16555/j.1006-8775.2014.04.009, 2014.

475

480

485

490

Table 1. The spatial standard deviation of SIC anomalies σ_{SIC} and shortwave radiation anomalies due to albedo effect $\sigma_{SW\text{-}albedo}$ (Wm^{-2}) over the Arctic Ocean. $r_{SW\text{-}albedo}$ is correlation coefficient between SIC and shortwave radiation anomalies. Those significant at 99% confidence level are bolded.

	Jan	Feb	Mar	Apr	May	Jun	Jul	Aug	Sep	Oct	Nov	Dec
σ_{SIC}	0.44	0.44	0.44	0.43	0.43	0.39	0.34	0.36	0.39	0.38	0.40	0.43
$\sigma_{SW\text{-}albedo}$	0.03	1.55	11.09	42.79	88.43	80.37	41.88	29.85	15.06	3.59	0.20	0
$r_{SW\text{-}albedo}$	-0.25	-0.43	**-0.75**	**-0.88**	**-0.90**	**-0.91**	**-0.90**	**-0.93**	**-0.88**	**-0.50**	-0.25	/

495

Table 2. The spatial standard deviation of shortwave and longwave radiation anomalies due to cloud change $\sigma_{SW\text{-}cloud}$, $\sigma_{LW\text{-}cloud}$ (Wm^{-2}) and water vapour change $\sigma_{SW\text{-}wv}$, $\sigma_{LW\text{-}wv}$(Wm^{-2}) over the Arctic Ocean. $r_{SW\text{-}cloud}$, $r_{LW\text{-}cloud}$, $r_{SW\text{-}wv}$ and $r_{LW\text{-}wv}$ are correlation coefficients between SIC and shortwave and longwave radiation anomalies due to cloud and water change respectively. Those significant at 99% confidence level are bolded. Here the cloud and water vapour change is specified as the part caused by sea-ice decrease.

|	Annual	Jan	Feb	Mar	Apr	May	Jun	Jul	Aug	Sep	Oct	Nov	Dec
$\sigma_{SW\text{-}cloud}$	4.86	0.01	0.16	1.20	4.56	6.84	12.53	19.14	14.45	4.16	0.65	0.04	0
$r_{SW\text{-}cloud}$	0.31	0.15	0.27	0.41	0.42	0.29	0.19	0.21	0.35	0.40	0.37	0.32	/
$\sigma_{LW\text{-}cloud}$	8.25	8.89	9.19	8.13	7.96	10.73	11.81	14.06	13.55	13.64	11.31	10.31	9.83
$r_{LW\text{-}cloud}$	**-0.52**	**-0.58**	**-0.59**	**-0.58**	**-0.55**	**-0.45**	-0.09	-0.07	-0.33	**-0.62**	**-0.52**	**-0.64**	**-0.58**
$\sigma_{SW\text{-}wv}$	0.27	0.001	0.03	0.14	0.38	0.57	0.79	0.77	0.56	0.28	0.08	0.01	0
$r_{SW\text{-}wv}$	-0.07	-0.08	-0.03	0.01	-0.01	-0.06	0.06	-0.08	**-0.49**	**-0.56**	-0.44	-0.24	/
$\sigma_{LW\text{-}wv}$	2.23	3.40	3.46	3.07	2.80	2.51	2.53	1.92	1.55	1.58	2.21	2.96	3.61
$r_{LW\text{-}wv}$	**-0.62**	**-0.50**	**-0.48**	**-0.56**	**-0.62**	**-0.60**	**-0.48**	-0.12	0.33	-0.06	**-0.52**	**-0.67**	**-0.57**

500

505

Table 3. The spatial standard deviation of sensible and latent heat flux anomalies σ_{SH}, σ_{LH} (Wm^{-2}) over the Arctic Ocean. r_{SH} and r_{LH} are correlation coefficients between SIC and sensible and latent heat flux anomalies respectively. Those significant at 99% confidence level are bolded.

	Jan	Feb	Mar	Apr	May	Jun	Jul	Aug	Sep	Oct	Nov	Dec
σ_{SH}	28.53	29.44	21.64	12.87	7.94	9.46	9.55	2.63	2.11	7.02	31.11	26.80
r_{SH}	**0.57**	**0.64**	**0.67**	**0.66**	**0.76**	0.26	-0.36	0.03	**0.65**	**0.80**	**0.71**	**0.56**
σ_{LH}	18.70	19.00	14.75	9.46	5.64	5.84	8.75	1.93	1.69	5.77	19.87	17.44
r_{LH}	**0.74**	**0.77**	**0.78**	**0.76**	**0.71**	0.14	-0.42	-0.37	**0.69**	**0.90**	**0.79**	**0.72**

510

Table 4. The response coefficients (Wm^{-2}) of radiation and turbulent heat fluxes to the albedo and insulation effects of sea-ice. Those significant at 99% confidence level are bolded.

λ (Wm^{-2})	flux		Ann	Jan	Feb	Mar	Apr	May	Jun	Jul	Aug	Sep	Oct	Nov	Dec
albedo	SW		**-46.5**	0.0	-1.7	**-18.9**	**-87.2**	**-188.1**	**-186.0**	**-109.7**	**-77.5**	**-34.4**	**-4.7**	-0.1	0
insulation	SW	cloud	4.3	0.0	0.1	1.1	4.4	4.6	6.1	11.3	13.7	4.2	0.6	0.0	0
		WV	-0.1	0.0	0.0	0.0	0.0	-0.1	0.1	-0.2	**-0.7**	**-0.4**	-0.1	0.0	0
	LW	cloud	**-12.6**	**-11.9**	**-12.2**	**-10.8**	**-10.0**	**-11.4**	-2.7	-2.8	-12.2	**-21.3**	**-15.2**	**-16.4**	**-13.6**
		WV	**-4.0**	**-3.9**	**-3.8**	**-3.9**	**-4.0**	**-3.6**	**-3.1**	-0.7	1.4	-0.3	**-3.0**	**-5.0**	**-4.8**
	SH		**35.3**	**53.4**	**59.0**	**46.4**	**29.6**	**24.2**	10.4	-13.8	0.4	**7.1**	**22.3**	**79.2**	**54.0**
	LH		**27.7**	**45.3**	**46.0**	**36.6**	**25.0**	**16.1**	3.5	-15.0	-3.6	**6.0**	**20.5**	**56.7**	**45.7**
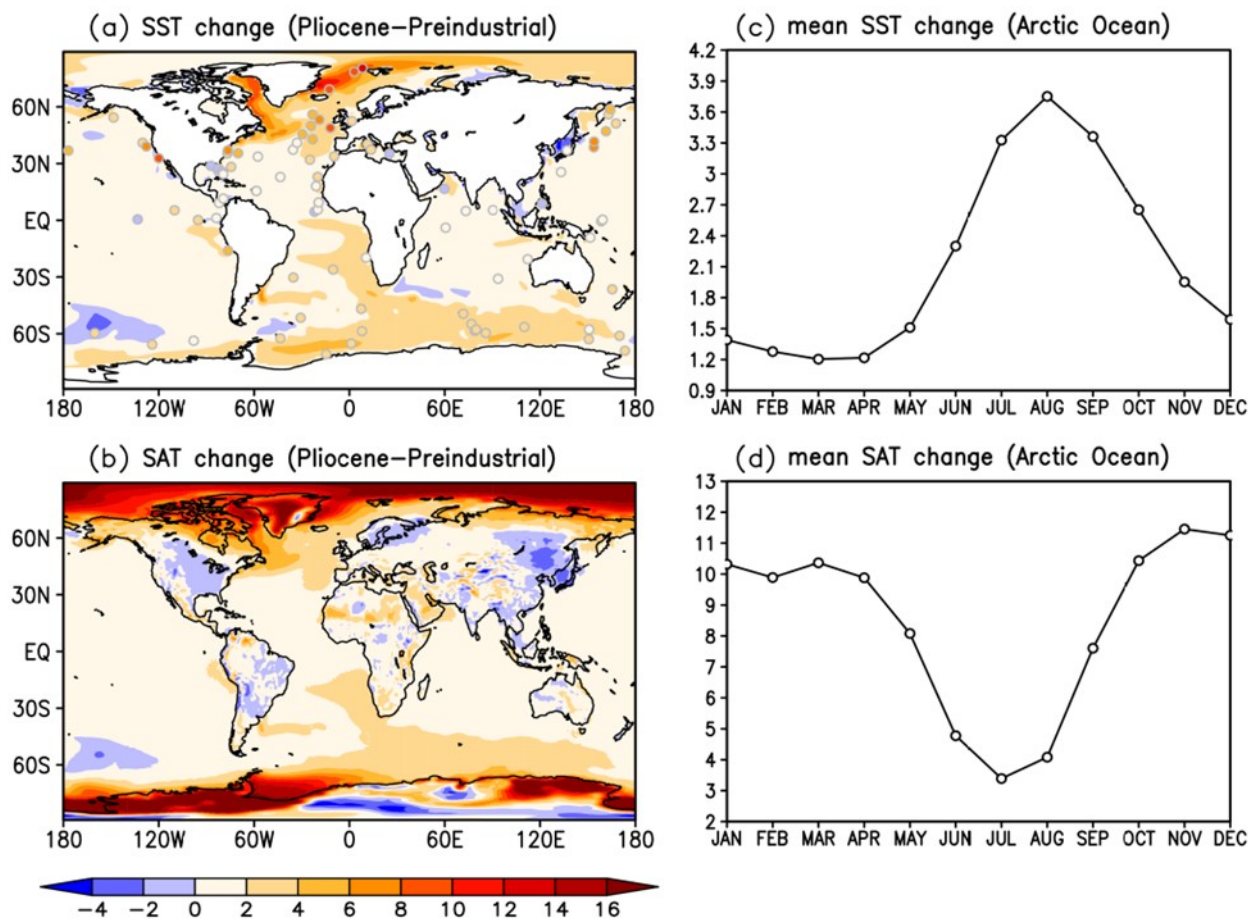
Figure 1. The annual mean warming (K) for (a) sea surface temperature (SST), (b) surface air temperature (SAT) and seasonal warming (K) averaged over the Arctic Ocean for (c) SST, (d) SAT between the Pliocene and preindustrial simulations. The shaded circles in (a) represent the annual mean SST anomalies at 95% confidence-assessed marine sites from Deep Sea Drilling Project (DSDP) and Ocean Drilling Program (ODP).
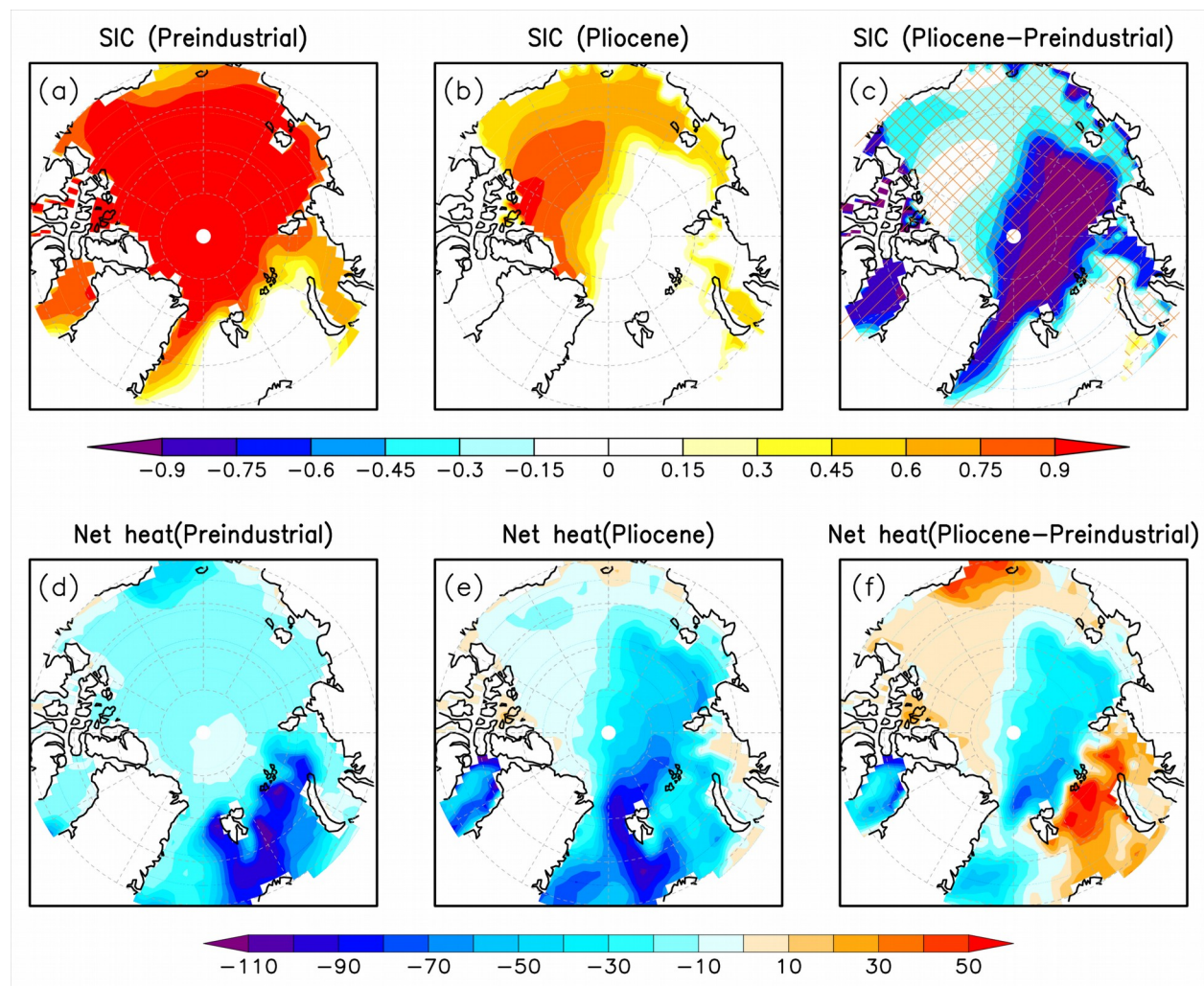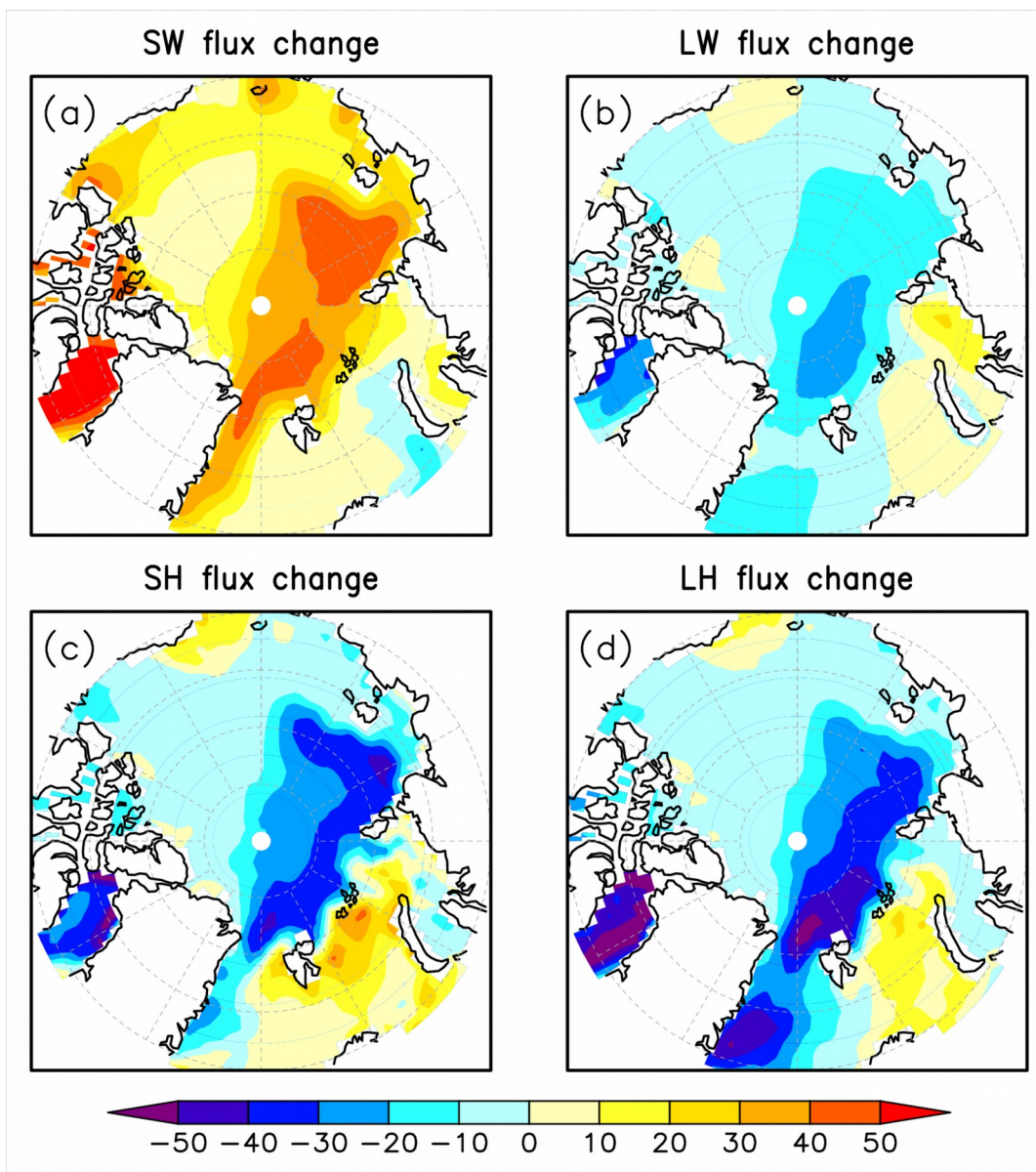
Figure 2. Spatial distributions of the annual mean sea-ice concentration (SIC) and air-sea interface net heat flux (Wm^{-2}, positive downward) over the Arctic Ocean. (a) SIC in the preindustrial, (b) SIC in the Pliocene, (c) the Pliocene SIC change with respect to the preindustrial, (d) net heat flux in the preindustrial, (e) net heat flux in the Pliocene, (f) the Pliocene net heat flux change with respect to the preindustrial. The diagonal stripe in (c) represents the regions from ice-covered to ice-free, and the diagonal crosshatch represents the regions from ice-covered to ice-covered.
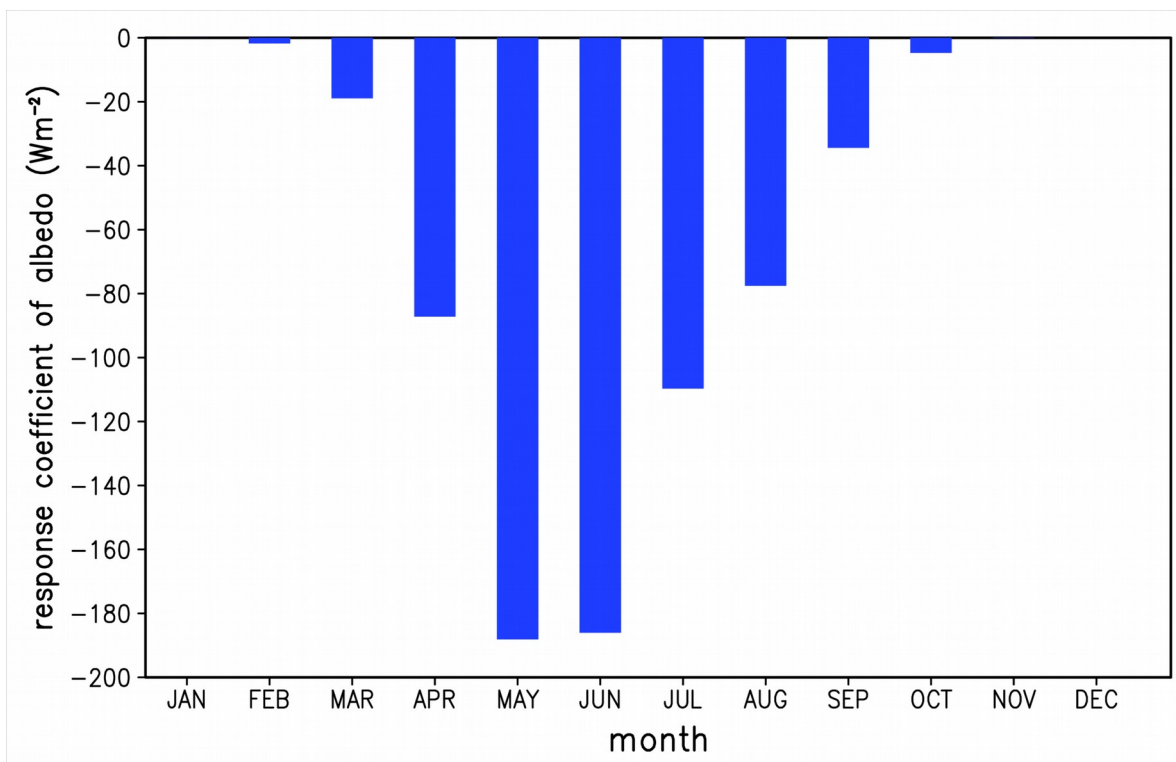
Figure 3. Spatial distributions of the Pliocene annual mean heat flux change (Wm^{-2}, positive downward) with respect to the preindustrial over the Arctic Ocean. (a) shortwave radiation flux, (b) longwave radiation flux, (c) sensible heat flux, (d) latent heat flux.

535

Climate
of the Past
Discussions

Open Access

EGU
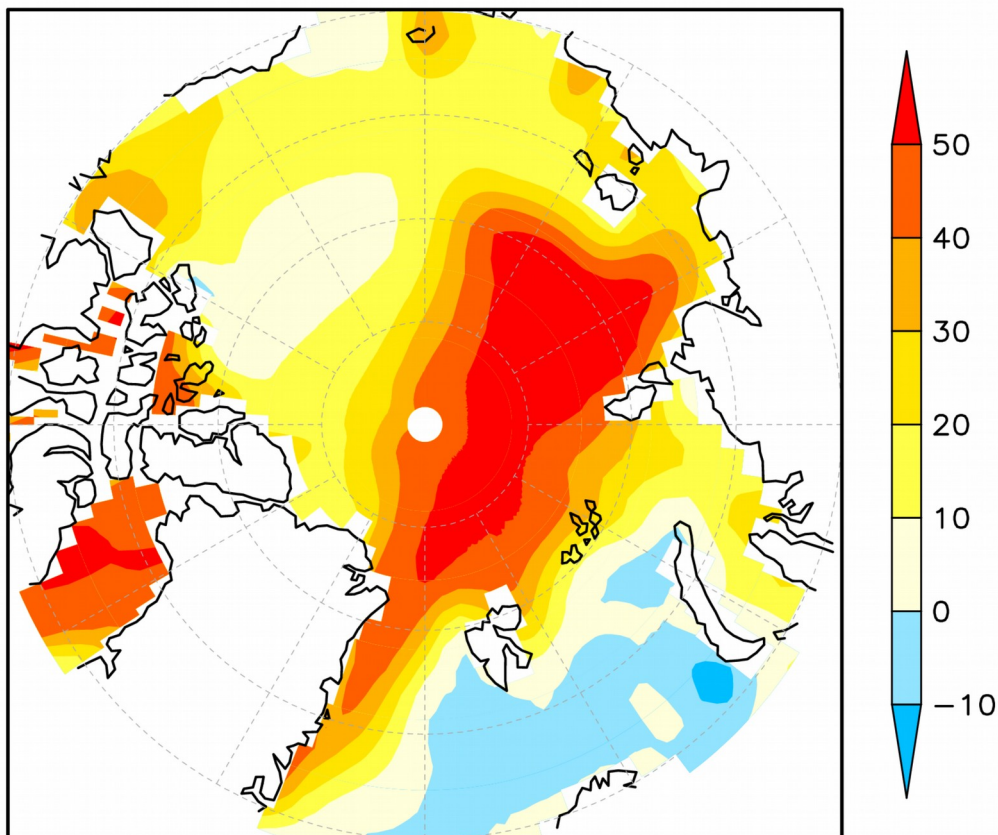
Figure 4. Spatial distributions of the Pliocene annual mean shortwave radiation flux change (Wm^{-2}, positive downward) over the Arctic Ocean caused by albedo effect of sea-ice change with respect to the preindustrial.

540

545
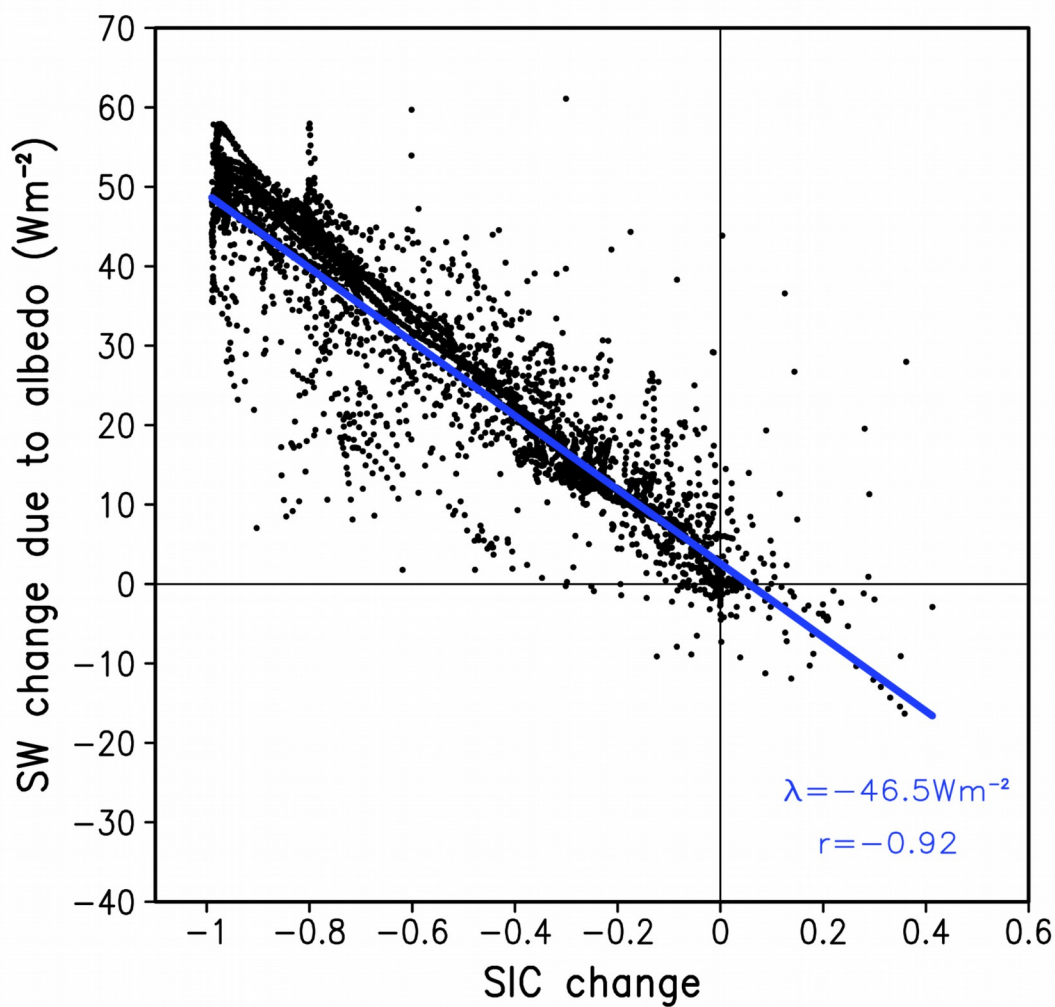
Figure 5. The annual mean shortwave radiation flux change (Wm^{-2}, positive downward) caused by albedo effect of sea-ice change averaged over the Arctic Ocean as a function of SIC change. All the change are with respect to the preindustrial.

Figure 6. The monthly response coefficients (Wm^{-2}) of shortwave radiation flux to the albedo effect of sea-ice.

560

565
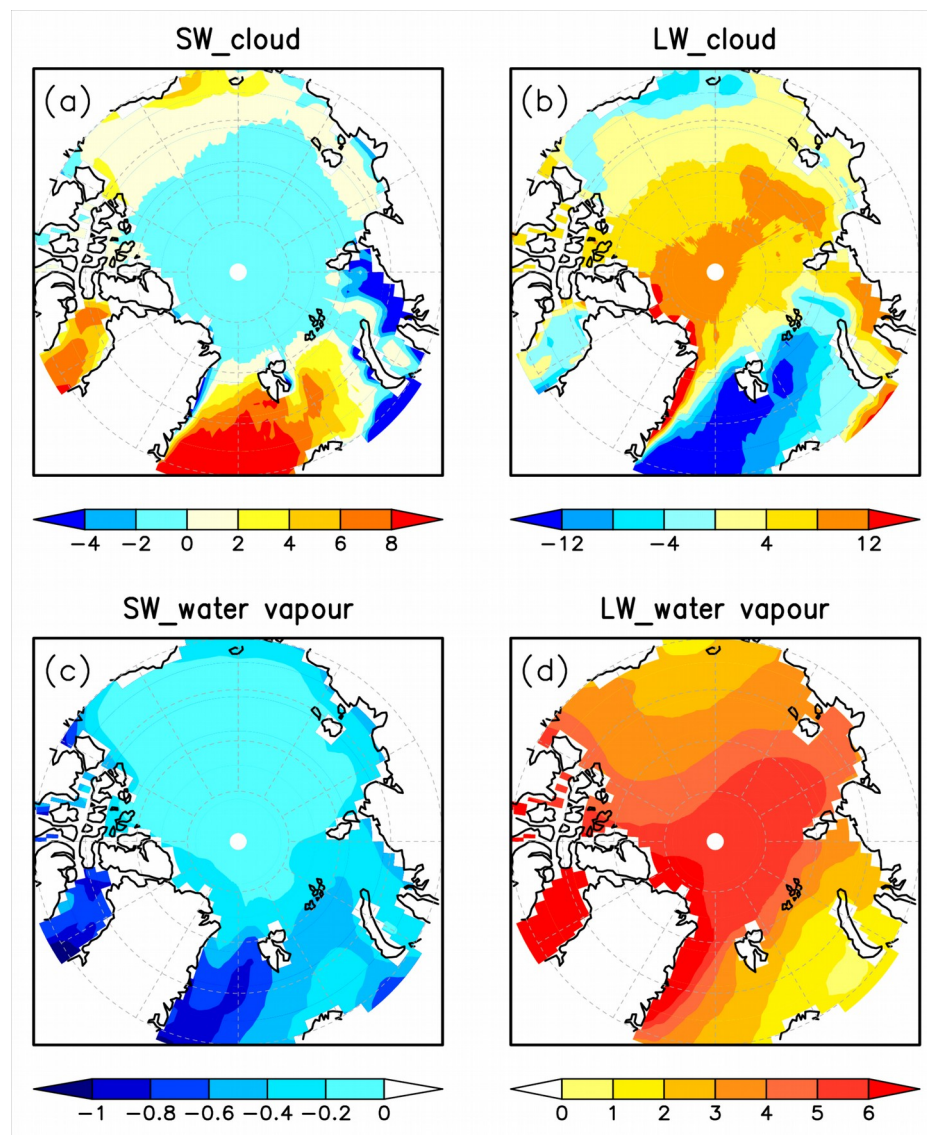
Figure 7. Spatial distributions of the Pliocene annual mean radiation fluxes change (Wm^{-2}, positive downward) with respect to the preindustrial over the Arctic Ocean. (a) shortwave radiation due to cloud change, (b) longwave radiation due to cloud change, (c) shortwave radiation due to water vapour change, (d) longwave radiation due to water vapour change. Here the cloud and water vapour change is specified as the part caused by sea-ice decrease.
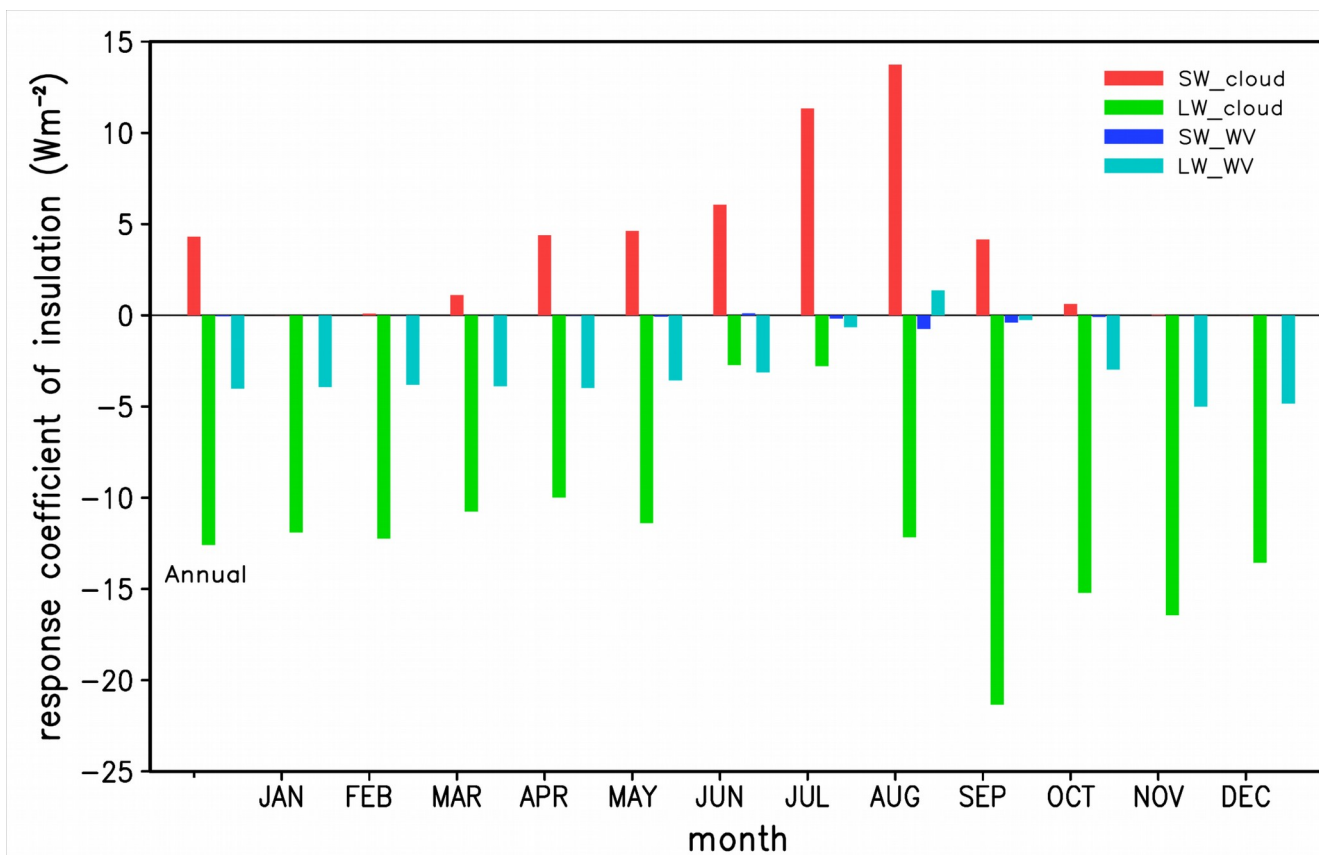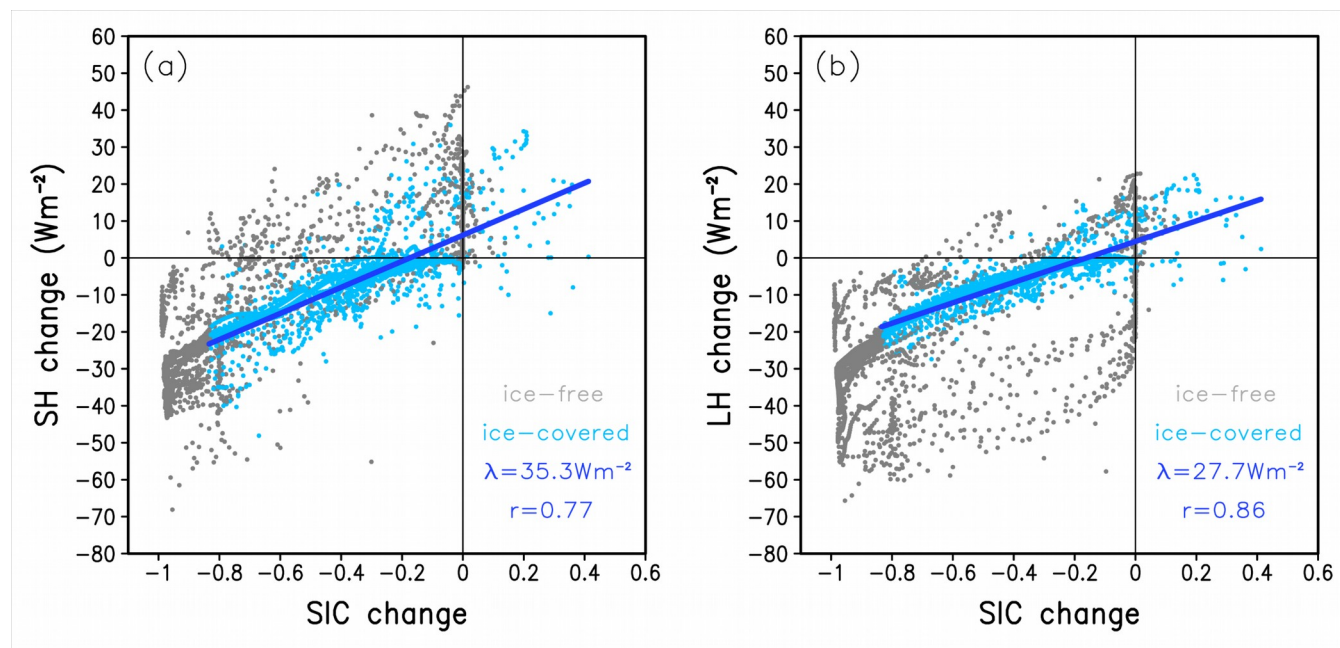
Figure 8. The annual and monthly response coefficients (Wm^{-2}) of shortwave and longwave radiation flux caused by cloud and water vapour change to the insulation effect of sea-ice. Here the cloud and water vapour change is specified as the part caused by sea-ice decrease.
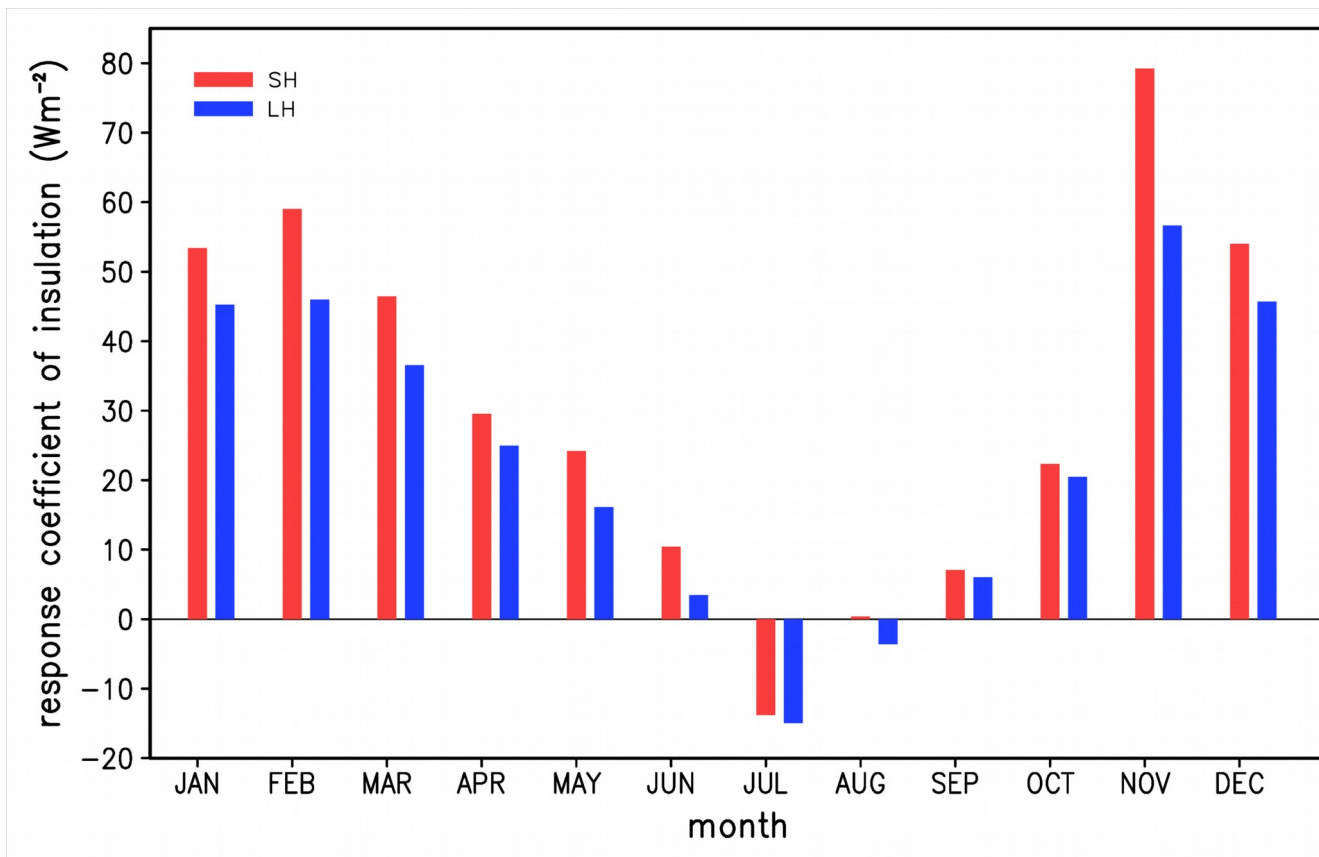
Figure 9. The annual mean sensible and latent heat flux change (Wm⁻², positive downward) caused by insulation effect of sea-ice change
595 averaged over the Arctic Ocean as a function of SIC change. All the change are with respect to the preindustrial.

600

605

Figure 10. The monthly response coefficients (Wm^{-2}) of sensible and latent heat fluxes to the insulation effect of sea-ice.